Available online at www.sciencedirect.com
SCIENCE DIRECT®
Journal of Organometallic Chemistry 690 (2005) 482–492
Journal of Organometallic Chemistry
www.elsevier.com/locate/jorganchem

Molecular conformations and π-hydrogen bonds in *anti*- and *syn*-binuclear Rh(I) complexes of *as*-indacene-diide: a computational study

Laura Orian, Paolo Ganis, Saverio Santi *, Alberto Ceccon

Dipartimento di Scienze Chimiche, Universitá degli Studi di Padova, Via Marzolo 1, 35131 Padova, Italia

Received 19 June 2004; accepted 29 September 2004

Abstract

Ab initio calculations are employed to interpret the different conformations in mono- and bi-nuclear Rh(I) derivatives of *as*-indacene, observed by X-ray crystallography. In particular, we discuss the quite unusual COD (1,5-cyclooctadiene) group orientation in the homo-bimetallic complex *anti*-{2,7-dimethyl-*as*-indacene-diide-[Rh(COD)]$_2$}, which is related to the metal hapticity and is stabilised by the presence of π-hydrogen bonds between olefin protons of COD and the π-electron cloud of the six-membered ring of the bridging ligand. Finally, the structure of *syn*-{2,7-dimethyl-*as*-indacene-diide-[Rh(COD)]$_2$} is treated where mainly steric constraints appear to control the spatial disposition of the ancillary ligands. Second-order perturbative natural bond orbital (NBO) analysis provides a meaningful picture of non-covalent intramolecular C–H···C(π) interactions.

PACS: 31.15.Ar; 33.15.Bh; 31.15.Ew
Keywords: π-hydrogen bond ab initio calculations rhodium indacene

1. Introduction

Half-sandwich indacenyl (Ic) complexes, in which one or two metals are coordinated to the cyclopentadienyl (Cp) moieties of the bridging ligand, are interesting model systems for detailed studies on the cooperative effects and more in general electronic communication [1]. Recently, some of us synthesised monometallic rhodium derivatives of *s*- and *as*-hydroindacenide and bimetallic rhodium complexes of *s*- and *as*-indacene-diide [2–6]. Other research groups studied homo-binuclear complexes of Fe, Co, Ni, Mn, with the same aromatic 14-π-electron spacers [7–13], which have been identified as suitable bridging ligands in view of strong electronic interactions between the two coordinated metal centres. Moreover their structure assures a control of the distance and orientation between the metals which may be arranged in a *syn* or *anti* configuration with respect to the rigid bridge plane. Like indenyl (Ind) complexes, Ic derivatives display several structural features which may play important roles in their reactivity, i.e., sensitivity of the ring orientation to the other ligands, unequal metal-ring carbon distances (ring slippage) and distortion of the ring from pentagonal symmetry.

From a theoretical viewpoint, the quantitative prediction of these features is challenging, due to the molecular size and the presence of one or two heavy nuclei.

Several computational studies on Ind complexes [14–19] have been performed at semi-empirical level of theory, i.e., extended Huckel method (EHMO) [20], and by density-functional theory (DFT) approach [21],

* Corresponding author. Tel.: +390498275119; fax: +390498275-239.
E-mail address: s.santi@chfi.unipd.it (S. Santi).

0022-328X/$ - see front matter © 2004 Elsevier B.V. All rights reserved.
doi:10.1016/j.jorganchem.2004.09.078

which allowed to point out the role of steric and electronic effects in determining the structural parameters in series of mononuclear indenyl and bis-indenyl complexes [14–18,22,23]. The metals of these complexes belong mainly to groups 6–10.

A computational study on *s*- and *as*-Ic complexes of Fe, Co and Ni was presented by Manriquez and co-workers [24], who interpreted qualitatively the trends in the metal hapticity by EHMO calculations.

In this paper, we present several calculations on mono- and bi-nuclear half-sandwich Rh(I) derivatives of *as*-indacene with the ancillary ligand COD [3,4]. Starting from their X-ray structures, we describe a simplified conformational study based on DFT geometry optimisations and subsequent single point energy calculations at different levels of theory. We employ both full and partially constrained geometry optimisations, since the state of the art functional (B3LYP) and basis sets for rhodium overestimate the ring slippage, which is found to have a severe influence on the COD orientation.

In the second part of the paper, we focus on the crystallographic evidence of weak intramolecular C–H···C(π) interactions in the bimetallic isomeric Rh(I) complexes [25], in which very short distances between the COD olefin protons and the centroid of the six-membered ring of the bridging ligand have been measured, i.e. less than 2.5 Å.

It is well known and generally accepted that non-classical hydrogen bonding can form between an acidic C–H group, acting as a weak proton donor, and unsaturated carbon atoms or carbanions that can accept hydrogen bonds [26–29]. In particular, when the acceptor is a π moiety the resulting interaction, the so-called π-hydrogen bond [30], is one of the weakest C–H···C(π) interactions encountered, but it controls many self-assembly phenomena, such as crystal packing and three-dimensional folding of proteins [31–33].

C–H···C(π) interactions have been theoretically studied by Honda and co-workers [34] through high level ab initio calculations on intermolecular complexes formed by benzene and one hydrocarbon molecule, i.e., methane, ethane, ethylene or acetylene. From the shape of the potential energy surface, which is very flat near the minimum, they show that the major source of attraction is a long-range dispersive interaction, which is found by explicitly including electron correlation.

Kim and Tarakeshwar [35–37] applied the perturbational SAPT (symmetry adapted perturbation theory) method and provided a clear picture of the interaction forces between some π-hydrogen bonded complexes, such as NH_3-, H_2O-, HF-ethene, benzene-H_2O and benzene-$(H_2O)_2$. They point out the necessity of performing both geometry optimisations and energy calculations entirely at MP2 level of theory [38] at least, which reproduces to a large extent the results obtained using more sophisticated electron correlation methods, such as CCSD(T) [39,40].

Treatments at the same level of accuracy cannot be applied to large molecules containing one or more heavy atoms like transition metals since the computational cost would be enormous. The investigation of the weak intramolecular C–H···C(π) interactions in the bimetallic rhodium complexes is here performed through NBO analysis [41,42].

2. Computational details

All the calculations were carried out with GAUSSIAN98 program [43]. The B3LYP hybrid functional with a standard LANL2DZ-ECP basis set for rhodium and 6-31G** for C and H (B3LYP/LANL2DZ, 6-31G**) was used [44–49]. The B3LYP functional includes a mixture of Hartree–Fock exchange with DFT exchange correlation, given by Becke's three parameter functional, which includes both local and non-local terms. We performed both full geometry optimisations (denoted with subscript FO) and partially constrained geometry optimisations (denoted with subscript PO), i.e., keeping frozen the five distances rhodium–carbon atoms of the Cp ring. The minima were checked by frequency calculations. Different basis sets were also tested for rhodium, i.e., SDD-ECP1997 in the full optimisations of the mono- and *anti*-bi-nuclear complexes (B3LYP/SDD1997, 6-31G**), and LANL2-DZECP plus a s-type function (exponent 0.1 and contraction 1.0) in the full optimisation of the *anti*-bimetallic *as*-Ic complex (B3LYP/LANL2DZ+s, 6-31G**). Single point energies of selected geometries (see text) were calculated also at Hartree–Fock (RHF) and at the second-order Möller–Plesset (MP2) [38] levels of theory, employing LANL2DZ-ECP for rhodium atoms and 6-31G** basis set for H and C atoms. NBO analysis was performed at B3LYP level of theory with the package NBO 3.1 [50] included in GAUSSIAN98; LANL2DZ-ECP basis set was employed for rhodium, 6-311G** for C and H (B3LYP/LANL2DZ, 6-311G**).

On the organic complexes benzene–ethylene and ethylene–benzene–ethylene, geometry optimisations and single point energy values were both calculated at MP2/6-311G** level of theory. 6-31G and cc-PVTZ basis sets were also tested [49]. The interaction energy values were BSSE corrected according to Boys–Bernardi counterpoise scheme [51]. NBO analysis on the complex ethylene–benzene–ethylene was carried out at B3LYP level of theory, employing a 6-311G** basis set for H and C atoms (B3LYP/6-311G**). 6-311+G* and 6-311++G** basis sets were also tested for C and H.

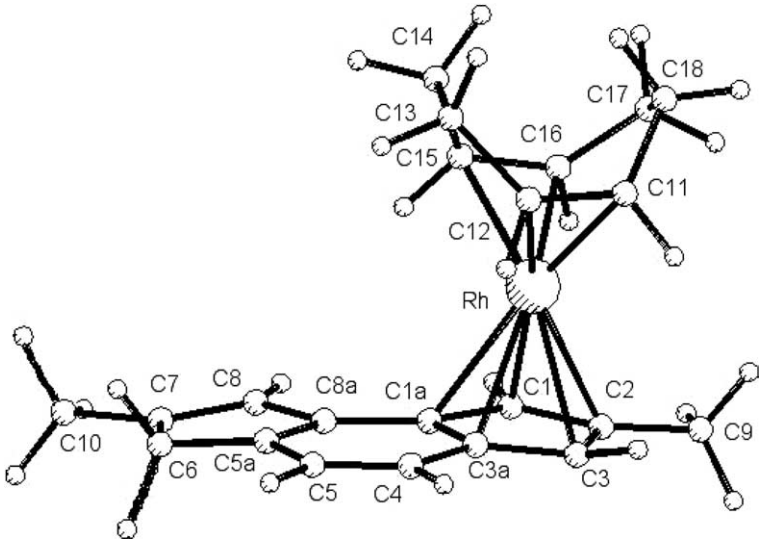

Fig. 1. Crystallographic molecular structure: 6-hydro-2,7-dimethyl-*as*-indacenide-Rh(COD) (*I*). The numbering scheme of the X-ray data is employed.

3. COD orientation in mono- and bi-nuclear Rh(I) complexes

A thorough treatment of the crystallographic properties of the monometallic complex 6-hydro-2,7-dimethyl-*as*-indacenide-Rh(COD) (Fig. 1) and of the complex *anti*-{2,7-dimethyl-*as*-indacene-diide-[Rh(COD)]$_2$} (Fig. 2) was presented by Ceccon and co-workers [3,4]. In the monometallic complex *I* (Fig. 1), it was shown that the two olefin double bonds of the ancillary ligand COD lie on planes almost parallel to the Ic moiety and are oriented in a direction almost orthogonal to the ring junction bond. The same COD orientation was observed also in Ind [52] and *s*-Ic monometallic complexes of rhodium and iridium [4,5].

On the contrary, the crystal structure of the *anti* bimetallic complex *II* (Fig. 2) shows a different orientation of the COD ligands: the two olefin double bonds of each COD still lie on planes almost parallel to that of the Ic moiety but they are unusually oriented with the double bonds almost aligned to the C_2-axis lying in the plane of the dianionic bridge. This conformational difference was in part explained in a previous communication [25] by invoking symmetry considerations.

Finally, in the isomer bimetallic complex *syn*-{2,7-dimethyl-*as*-indacene-diide-[Rh(COD)]$_2$} (III) (Fig. 3) the two different COD orientations are both present in the crystal structure [4]. In this case, steric repulsion was invoked to justify the absence of symmetry in the orientation of the ancillary ligands and the high hinge angles [1] observed at the *as*-Ic spacer.

We focus our attention on the monometallic and the *anti*-bimetallic complexes. The X-ray structures *I* and *II* were fully optimised at B3LYP/LANL2DZ, 6-31G** level of theory (see Section 2). For bond distances not involving the metal a good agreement with experiment is found. On the contrary, metal–Cp distances are overestimated and an enhanced metal slippage is found. [2] The relevant geometric parameters are presented in Tables 1 and 2. The same disagreement is encountered in fully optimised CpRh(COD) and IndRh(COD), whose data are provided as supplementary material. In particular, we observe that the errors of the calculated distances between rhodium and the junction carbon atoms (C1a, C3a, C5a and C8a) increase from 5% (CpRh(COD)), to 7% (IndRh(COD)), to 8% in the monometallic Ic complex and to 10% in the *anti* bimetallic Ic complex.

Moreover in complex *II* a rotation of about 70° of the ancillary ligands is observed at the end of the optimisation: COD double bonds become orthogonal to the C_2-axis of the bridging ligand. We tested two different basis sets for rhodium, i.e., SDD-ECP 1997 and LANL2DZ+s (see Section 2), without significative improvement of the final geometry: in fact the

[1] The hinge angle Ω is defined as the angle between the planes of C1, C2, C3 and C1a, C1, C3, C3a.

[2] McCullough and co-workers [53] have defined a similar disagreement as a general feature of calculations on piano stool Cp complexes with transition metals. They performed complete all electron geometry optimisations on several Cp complexes of Ru, Mo, Co and Rh with different ancillary ligands (CH_3, NO, NS, Cl, CO) using BLYP and BPW91 functionals with Gaussian basis sets of double-ζ valence plus polarisation quality. Their results are in large disagreement with the experimental data, in most of the cases outside the range of plausible relativistic contractions. They propose that the source of error might lie in the correlation potential, as well as in the lack of inclusion of relativistic effects.

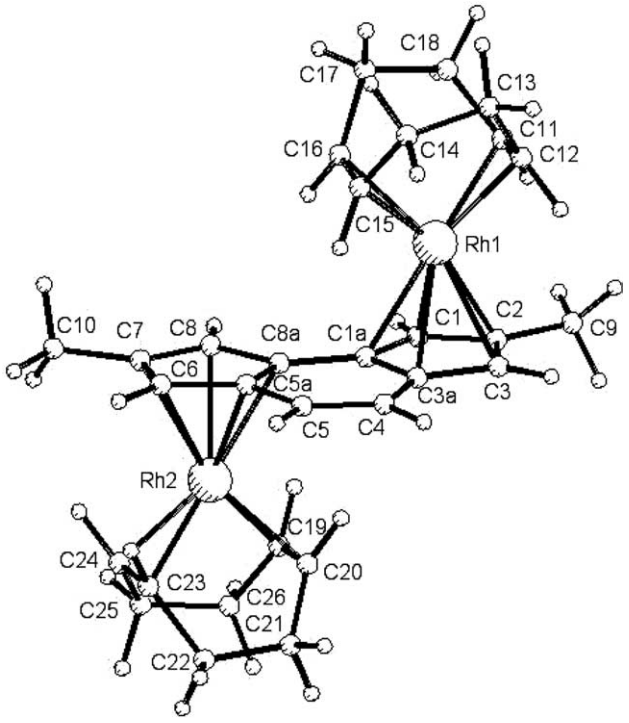

Fig. 2. Crystallographic molecular structure: *anti*-{2,7-dimethyl-*as*-indacene-diide-[Rh(COD)]$_2$} (*II*). The numbering scheme of the X-ray data is employed.

metal–Cp bond lengths are in better agreement with the experiments, but the final COD orientation in II_{FO} is in both cases rotated. These results presumably are due to: (i) the quality of the metal basis set, (ii) limitation of the correlation potential and (iii) neglect of relativistic effects [53]. In any case, the use of this computational state of the art method, i.e., B3LYP/LANL2DZ, 6-31G**, on these large complexes should be approached with due caution.

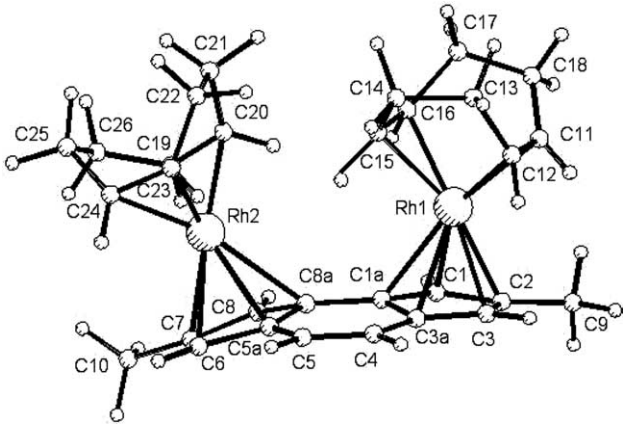

Fig. 3. Crystallographic molecular structure: *syn*-{2,7-dimethyl-*as*-indacene-diide-[Rh(COD)]$_2$} (*III*). The numbering scheme of the X-ray data is employed.

Table 1
Crystallographic and DFT optimised selected bond lengths (Å), angles (°) and slip distortion parameters Δ (Å) of 6-hydro-2,7-dimethyl-*as*-indacenide-Rh(COD)

	I[a]	I_{FO}[b]	I_{FO}[c]
Rh1–C1	2.220(7)	2.252	2.294
Rh1–C2	2.249(7)	2.280	2.322
Rh1–C3	2.224(6)	2.259	2.310
Rh1–C3a	2.375(6)	2.492	2.565
Rh1–C1a	2.371(6)	2.481	2.551
$d_{Rh1\text{-}Q}$[d]	1.968	2.011	2.072
Rh1–M1[e]	2.001	2.034	2.054
Rh1–M2[e]	2.022	2.035	2.059
∠M1–Rh1–M2[e]	87.3	87.6	87.4
Δ[f]	0.15	0.185	0.256

[a] Crystallographic data; standard deviations, when available, are indicated.
[b] Fully optimised geometry at B3LYP/SDD1997, 6-31G** level.
[c] Fully optimised geometry at B3LYP/LANL2DZ, 6-31G** level.
[d] Q denotes the centroid of the Cp moiety.
[e] M1 and M2 denote the middle points of COD olefin bonds.
[f] Δ values were calculated referring to the couples of atoms C3a–C1a and C1–C3: $\Delta = 0.5 \cdot (M\text{–}C1a + M\text{–}C3a) - 0.5 \cdot (M\text{–}C1 + M\text{–}C3)$ [54].

In complex *II*, the metal hapticity forces the COD orientation. Due to the numerous degrees of freedom of these molecules and the presence of one or two heavy nuclei, a full conformational study is unfeasible. Two coordinates are relevant: the orientation of the Rh-COD fragment, which can rotate about the ideal axis passing through rhodium and the estimated centre of the five-membered ring, and the Cp–metal bonding arrangement, i.e., the slippage of rhodium over the Cp ring. Thus, in order to discuss the effect of the rhodium hapticity on the conformation of COD in the monometallic complex and in the *anti*- bimetallic complex, their X-ray structures were partially optimised at B3LYP/LANL2DZ, 6-31G** level of theory (see Section 2), i.e., by keeping frozen the distances between the rhodium atoms and the five Cp carbon atoms, so that the exact crystallographic hapticity $\eta^3 + \eta^2$ of the metal was retained. By imposing this constraint, we allow the COD groups just to rotate and to move further or nearer from/to the plane of the bridging ligand.

The relevant geometric parameters of the partially optimised structures, I_{PO} and II_{PO}, are reported in Table 3. Partially constrained geometries exhibit the same COD orientation detected in the crystal state and the distances and angles involving the metal and the COD ligands are in good agreement with the crystallographic data. In particular, I_{PO} and II_{PO} are not only the molecular structures in better agreement with the crystallographic results, but also resemble quite well the molecular conformations dominating in solution, as a very recent combined experimental and DFT study on ^{103}Rh NMR chemical shifts has confirmed [55].

Table 2
Crystallographic and DFT optimised selected bond lengths (Å), angles (°) and slip distortion parameters Δ (Å) of *anti*-{2,7-dimethyl-*as*-indacene-diide-[Rh(COD)]$_2$}

	II[a]	**II$_{FO}$**[b]	**II$_{FO}$**[c]	**II$_{FO}$**[d]
Rh1–C1	2.277(8)	2.259	2.305	2.276
Rh1–C2	2.243(9)	2.287	2.331	2.304
Rh1–C3	2.28(1)	2.262	2.308	2.276
Rh1–C3a	2.30(1)	2.470	2.537	2.510
Rh1–C1a	2.252(9)	2.460	2.525	2.500
d_{Rh1-Q}[e]	1.920	2.005	2.063	2.036
Rh1–M1[f]	1.997	2.030	2.052	2.048
Rh1–M2[f]	2.007	2.030	2.050	2.047
∠M1–Rh1–M2[f]	87.8	87.5	87.4	87.3
Δ[g]	0.00[h]	0.204	0.224	0.229
Rh2–C8	2.30(1)	2.259	2.305	2.277
Rh2–C7	2.28(1)	2.287	2.330	2.304
Rh2–C6	2.26(1)	2.262	2.307	2.276
Rh2–C5a	2.288(8)	2.471	2.538	2.510
Rh2–C8a	2.243(9)	2.460	2.527	2.501
$d_{Rh2-Q'}$[e]	1.915	2.005	2.063	2.036
Rh2–M1′[f]	2.006	2.029	2.052	2.048
Rh2–M2′[f]	1.997	2.030	2.050	2.046
∠M1′–Rh2–M2′[f]	87.3	87.5	87.4	87.3
Δ[g]	−0.02[h]	0.205	0.224	0.229

[a] Crystallographic data; standard deviations, when available, are indicated.
[b] Fully optimised geometry at B3LYP/SDD1997, 6-31G** level.
[c] Fully optimised geometry at B3LYP/LANL2DZ, 6-31G** level.
[d] Fully optimised geometry at B3LYP/LANL2DZ+s, 6-31G** level.
[e] Q and Q′ denote the centroids of the Cp moiety.
[f] M1, M2, M1′ and M2′ denote the middle points of COD olefin bonds.
[g] Δ values were calculated referring to the couples of atoms C3a–C1a (C5a–C8a) and C1–C3 (C6–C8): $\Delta = 0.5 \cdot (M\text{–}C1a + M\text{–}C3a) - 0.5 \cdot (M\text{–}C1 + M\text{–}C3)$ [54].
[h] In complex II$_{PO}$, zero and negative values are due to the fact that the distances Rh1–C1a and Rh2–C8a are uncommonly short and the typical slippage towards C2 and C7 is not encountered [4].

The different stability of II$_{FO}$ and II$_{PO}$ reflects the stability of their HOMOs (Fig. 4). In both cases, the metal fragments are disposed in anti-bonding fashion with respect to the bridging ligand. In II$_{PO}$, the HOMO derives from the HOMO − 1 of indacene dianion of symmetry b (C_2 symmetry labels are employed) with two contributions from a filled and an empty orbital of the metallic fragments with rhodium d_{xz} and d_{yz} character. In II$_{FO}$, the HOMO is principally derived from the HOMO and HOMO − 2 of indacene dianion, both of symmetry a [24], with two contributions from a filled and an empty orbital of the metallic fragments with rhodium d_{x2-y2} and d_{xz} character.

Table 3
Selected bond lengths (Å) and angles (°) of partially optimised geometries of 6-hydro-2,7-dimethyl-*as*-indacenide-Rh(COD) and *anti*-{2,7-dimethyl-*as*-indacene-diide-[Rh(COD)]$_2$}

	I$_{PO}$[a]	**II$_{PO}$**[a]
Rh1–M1[b]	2.067	2.049
Rh1–M2[b]	2.062	2.043
∠M1–Rh1–M2[b]	87.0	86.7
Rh2–M1′[b]		2.046
Rh2–M2′[b]		2.040
∠M1′–Rh2–M2′[b]		86.7

[a] Values referring to partially constrained optimised geometry (B3LYP/LANL2DZ,6-31G**), i.e., with imposed crystallographic $\eta^3 + \eta^2$ Rh–Cp coordination.
[b] M1, M2, M1′ and M2′ denote the middle points of COD olefin bonds.

Finally, in order to exclude dominant packing effects on the orientation of the ancillary ligands, starting from the optimised geometries I$_{PO}$ and II$_{PO}$, an anticlockwise rotation of each COD group about the ideal axis passing through rhodium and the estimated centre of the Cp ring, was performed (about 70°) and we obtained two unnatural complexes in which the COD group is anomalously disposed: in the monometallic complex the cyclooctadiene ring is oriented in the same fashion as the two COD groups of the structure II$_{PO}$ and vice versa. At the end of the constrained geometry optimisations, the COD groups show their original correct position in both cases, confirming that packing forces play a minor influence on the orientation of the ancillary ligands and that preserving the crystallographic hapticity, also the experimental COD orientation is retained.

The relative energies of selected couples of mono- and *anti*-bimetallic geometries are useful to inspect the different stability of the molecular models above described and are reported in Table 4. RHF and MP2 calculations [38] were also carried out and are shown in Table 4. RHF results are in agreement with the B3LYP stability trend: the full optimised geometries, which are characterised by an enhanced rhodium slippage, are the most stable.

The MP2 results for the couples I$_{FO}$/I$_{PO}$ and II$_{FO}$/II$_{PO}$ are in disagreement with RHF and B3LYP stability trend, I$_{PO}$ and II$_{PO}$ being more stable than I$_{FO}$ and II$_{FO}$, as found experimentally. The inclusion of explicit electron correlation lowers significantly the energy of complexes I$_{PO}$ and II$_{PO}$, suggesting that dispersive interactions, which are not taken into account in RHF calculations and are not efficiently described by B3LYP, might have an important stabilising role in these Rh(I)–Ic complexes.

It is worth noting that in both I$_{PO}$ and II$_{PO}$ complexes the positions of the carbon atoms in the molecular backbone are almost unchanged, but displacements of the COD olefin hydrogen atoms occur. In particular, in complex II$_{PO}$, in the region of the π-hydrogen bonds, the distances of C15 and C20 from the centroid of the six-membered ring (Q) change from 3.306 and 3.381 Å (X-ray structure) to 3.422 and 3.440 Å (DFT optimised structure), whereas the distances of the hydrogens H15 and H20 from *Q* increase from 2.405 to 2.796 Å, and from 2.448 to 2.805 Å, respectively. The corresponding angles C15–H15–Q and C20-H20-Q decrease by 28.0°

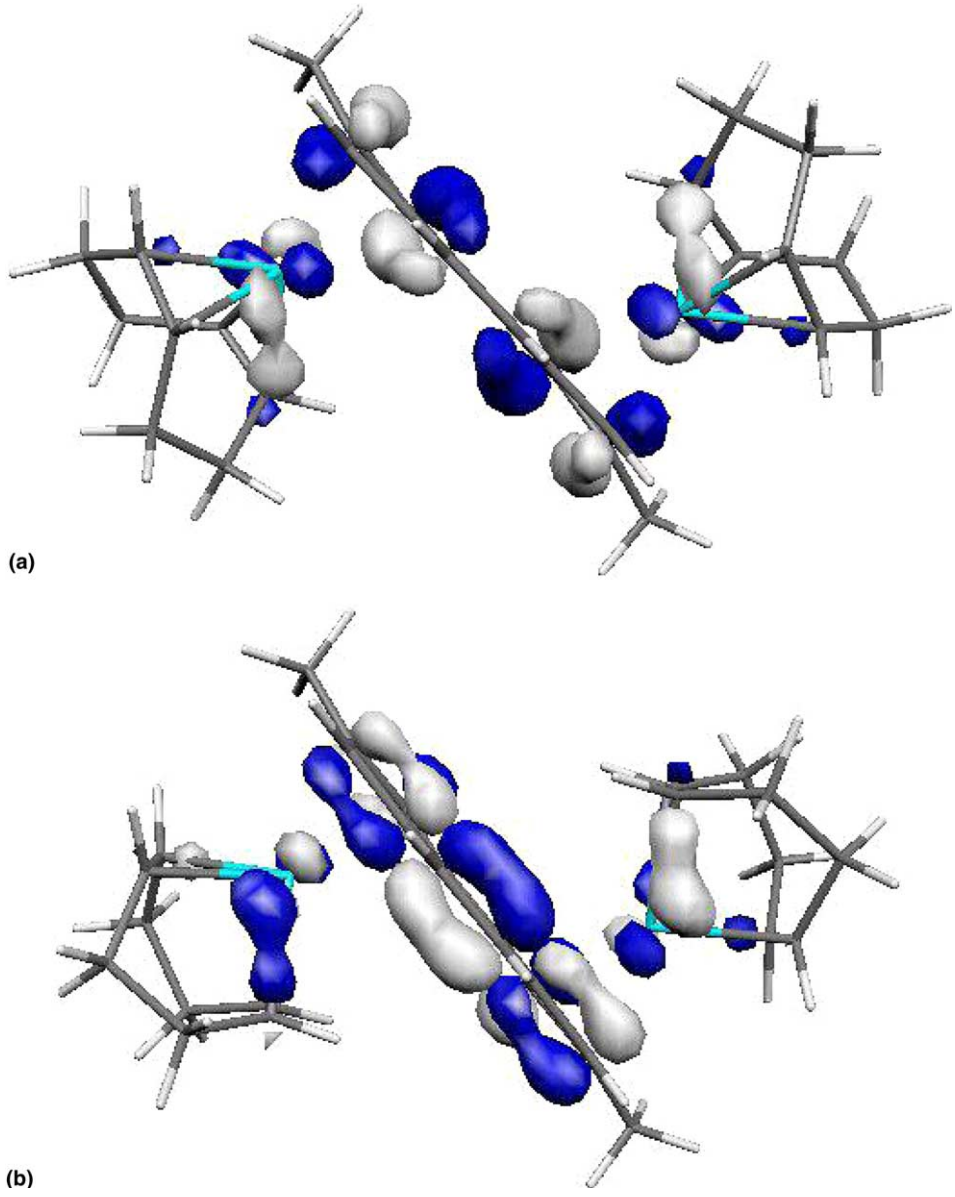

Fig. 4. Kohn–Sham highest occupied molecular orbitals (HOMOs) of II_{FO} (a) and II_{PO} (b).

and 23.0° respectively. Also in this regard the poor performance of the DFT method might be ascribed to the evidence that currently employed functionals scarcely describe dispersive interactions, such as π-hydrogen bonds [56]. The overestimated distance values found in DFT results are slightly shorter than the sum of the van der Waals radii for carbon and hydrogen (~2.90 Å), but no definite cut-off value for the C–H···C(π) bonding can be taken as a limit value [57], due to the long-range nature of the interaction, as it is illustrated in a recent database study specifically devoted to transition metal compounds [58].

Moreover, also the C–H···C(π) angle determines the strength of the interaction [57] and the energy minimum is found when the C–H bond points to the ring centre and the angle C–H–Q approaches 180°. Deviations from this ideal bonding geometry are experimentally observed in most of the molecules where π-hydrogen bonding is present, because the energy surface is very shallow, so that distortions from linearity have small effects on the energy. The number of possible structures for a bent C–H···C(π) geometry is much larger than for a linear arrangement [57,58].

Geometry optimisation at B3LYP/LANL2DZ, 6-31G** level was performed also on the *syn* isomer bimetallic complex, under the constraint of frozen metal hapticity (data are provided as supplementary material). The crystallographic distance between H15 and Q is 2.644 Å, but after geometry optimisation it increases dramatically to 3.374 Å, since a partial rotation of about

Table 4
Energy differences of couples of Rh(I) indacenyl complexes. All values are kcal mol^{-1}

	B3LYP	MP2	HF
I_{FO}–I_{PO}	−1.73	+4.23	−3.18
II_{FO}-II_{PO}	−10.33	+6.77	−11.72

10° of COD group is involved, probably due to the steric hindrance of the ancillary ligands.

4. Intramolecular π-hydrogen bonding and Natural Bond Orbital analysis

The energetic contribution of the π-hydrogen interactions is not isolable in the *anti* binuclear complex. Single point energy calculations provide only qualitative information on the stability of the different geometries. However, more in general, in the case of intramolecular C–H···C(π) bonding, the correspondent net energy is always shaded by other more relevant energy terms.

Thus we investigated the peculiar and uncommon feature of the *anti* bimetallic complex, i.e., the presence of two π-hydrogen bonds, one facing each other in the opposite sides of the benzene moiety, by employing a simplified model intermolecular complex. We calculated the interaction energies at equilibrium interatomic distances in neutral model complexes formed by one/two ethylenes riding a benzene on opposite sides (EB and EBE), as shown in Fig. 5. In this case, both geometry optimisations and single point energies were calculated at MP2/6-311G** level of theory. While at HF level in both complexes a energy plateau is reached when the distance between H and the centroid of the benzene ring exceeds 3.0 Å, at MP2 level a energy minimum is encountered at a distance of 2.6 Å (Fig. 5). The basis set dependence of HF interaction is very small, while the MP2 interaction energy depends greatly on the basis set. Small basis sets lead to the underestimation of molecular polarizability and dispersion interaction. The results obtained with the cc-PVTZ basis set for selected distances near the minimum are almost indistinguishable from those obtained with 6-311G**. A different result is instead obtained with the smaller 6-31G basis set at MP2 level: no minimum is encountered at 2.6 Å. The results are shown in Fig. 5. It should be noted that at the equilibrium distance (2.6 Å) the complexation energy of the two ethylenes with benzene (−5.63 kcal mol^{-1}) is slightly less than twice the complexation energy of the single ethylene with benzene (−2.91 kcal mol^{-1}) at the employed level of theory. There is no evidence of an *extra* stabilisation due to the presence of two protons

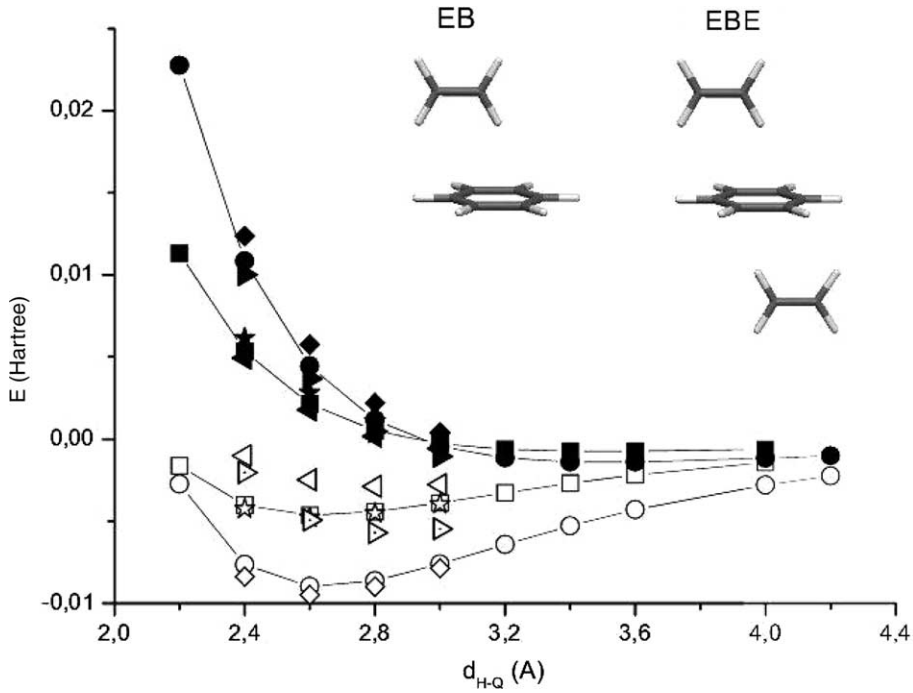

Fig. 5. Variation of the total interaction energy with the H–Q distance in the two intermolecular complexes EB and EBE at HF (filled symbols) and MP2 (open symbols) level of theory. For complex EB data calculated with 6-31G (left triangles), 6-311G** (squares) and cc-PVTZ (stars) basis sets are shown; for complex EBE data calculated with 6-31G (right triangles), 6-311G** (circles) and cc-PVTZ (diamonds) basis sets are shown. Energy values are BSSE corrected. Complexes EB and EBE are shown in the upper right corner.

pointing towards the same π aromatic cloud at the employed level of theory.

A direct analysis of intramolecular π-hydrogen bonding was performed on the basis of an easily accessible quantity useful to establish the presence of donor–acceptor interactions, i.e., NBO analysis [41,42]. NBO calculations provide a picture of localised bonds and lone pairs as basic units of the molecular structure. Each NBO is formed from orthonormal hybrid orbitals (NHO), which in turn are composed from a set of effective valence-shell atomic orbitals (NAO) optimised for the chosen wavefunction. There is a good agreement between NBO representations and Lewis structures. However the transformation to NBOs also leads to orbitals that are uncoupled in the formal Lewis structure and that may be used to describe non-covalency effects. These corrections to Lewis type picture are usually so small as to be approximated by second order perturbative expressions; the energy lowering is given by the formula:

$$\Delta E^{(2)} = -2\frac{\langle\sigma|\hat{F}|\sigma^*\rangle}{E_{\sigma^*} - E_{\sigma}}, \quad (1)$$

where $\hat{F}$ is the Fock operator and E_{σ^*} and E_{σ} are NBO orbital energies.

We completed our study performing the NBO analysis to verify the existence of donor–acceptor interactions between the C–H of the COD and the six membered ring of the bridging ligand. The analysis was performed on the crystallographic structures. In *anti*-{2,7-dimethyl-*as*-indacene-diide-[Rh(COD)]$_2$} we have found a bond-antibond interaction between $NBO_{C4–C5}$ and $NBO_{C15–H15}$ of 0.63 kcal mol^{-1} and between $NBO_{C4–C5}$ and $NBO_{C20–H20}$ of 0.12 kcal mol^{-1} (Fig. 6A). Interestingly the C–H$\cdots$C(π) interaction seems to involve only one π orbital of the six-membered ring, i.e., $NBO_{C4–C5}$. Although C4 and C5 are the most distant carbon atoms from H20 and H15, the stabilising interactions involve $NBO_{C4–C5}$. This can be explained on the basis of electronic factors. It is worth noting that in a

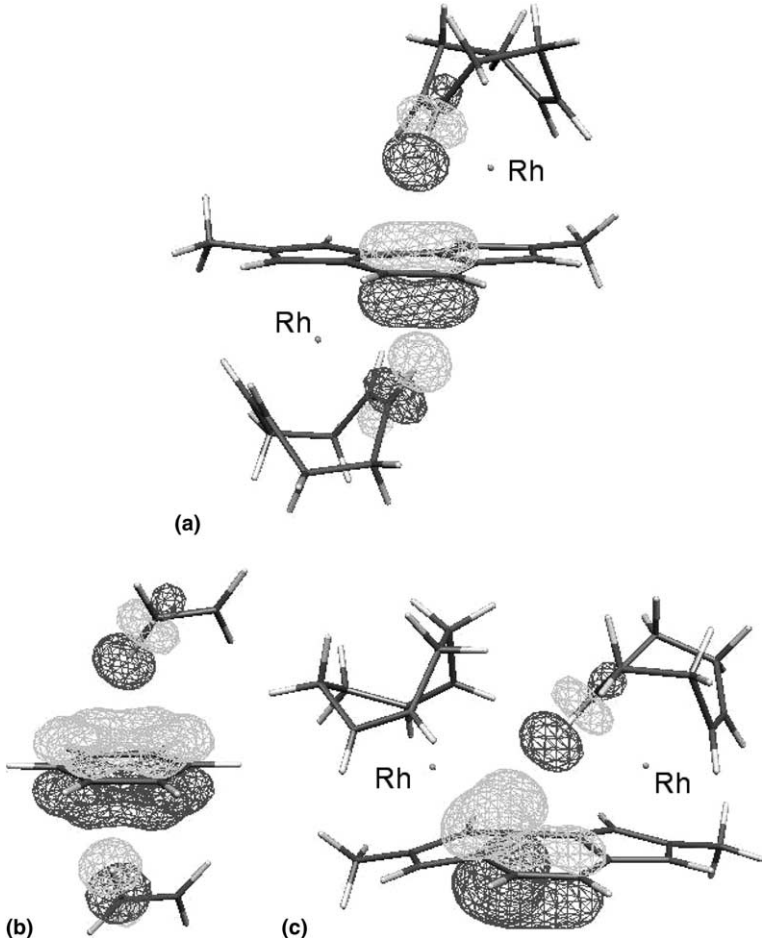

Fig. 6. $NBO_{C15–H15}$, $NBO_{C4–C5}$, $NBO_{C20–H20}$ (the numbering scheme is indicated in Fig. 2) calculated using the crystallographic structure of *anti*-{2,7-dimethyl-*as*-indacene-diide-[Rh(COD)]$_2$} (a); $NBO_{C15–H15}$, $NBO_{C20–H20}$, $NBO_{C4–C5}$, $NBO_{C5a–C8a}$ and $NBO_{C1a–C3a}$ (the numbering scheme is indicated in Fig. 2) calculated using the model complex ethylene-benzene-ethylene obtained from the crystallographic structure of *anti*-{2,7-dimethyl-*as*-indacene-diide-[Rh(COD)]$_2$} (b); $NBO_{C15–H15}$, $NBO_{C4–C5}$, $NBO_{C5a–C3a}$ (the numbering scheme is indicated in Fig. 3) calculated using the crystallographic structure of *syn*-{2,7-dimethyl-*as*-indacene-diide-[Rh(COD)]$_2$}.

previous communication [25] it was supposed that the best electronic structure of the 2,7-dimethyl-*as*-indacene-diide in the *anti*-bimetallic species has two negative charges localised on the Cp rings, so the 18 electron rule at the metal centers is obeyed, and a double bond is located between C4 and C5.

To verify that NBO analysis supports this electronic picture, we performed NBO analysis also on a model complex formed by a benzene ring and two ethylene molecules disposed on opposite sides over the faces with distances and orientation taken from the X-ray structure (Fig. 6B) of the *anti*-binuclear complex. The results are summarised in Table 5, where, for sake of simplicity, the same atomic labels of complex *II* are employed. The interaction is not symmetric also in this purely organic complex, since the molecular geometry is distorted, being the same as the *anti* bimetallic compound, but more energetic terms are found since benzene has a fully delocalised π cloud. This confirms that the intramolecular π-hydrogen interactions in complex *II* are of the so-called *edge* type [59], i.e., the C–H group interacts with only two adjacent carbons of the six-membered ring of the indacene-diide bridge. Similar intra-molecular contacts have already been observed in crystalline 2,6-diphenylphenol [60] and 4-nitro-2,6-diphenylphenol [61].

In Table 6, selected atomic charges and the natural populations calculated for complex *II* are reported. The difference in the natural population between the two adjacent olefin hydrogen atoms is small but in agreement with the presence of two intra-molecular π-hydrogen bonds in which H15 and H20 are involved.

NBO analysis was carried out also on the X-ray structure of the *syn*-binuclear complex (Fig. 6C). Two bond-antibond interactions in the NBO basis are found between $NBO_{C4–C5}$ (localised between C4 and C5) and $NBO_{C15–H15}$ (localised between C15 and H15) of 0.008 kcal mol^{-1} and between $NBO_{C5a–C3a}$ and $NBO_{C15–H15}$ of 0.013 kcal mol^{-1}. These extremely small energy values might be ascribed to the longer distance hydrogen-benzene in the *syn* isomer.

Table 5
Second order perturbative NBO analysis of a ethylene-benzene-ethylene complex whose structure is derived from complex *II* (see text)

Bonding (donor)	Anti-bonding (acceptor)	Energy (kcal mol^{-1})
$NBO_{C1a–C3a}$	$NBO_{C20–H20}$	0.12, 0.12[a], 0.13[b]
$NBO_{C4–C5}$	$NBO_{C20–H20}$	0.50, 0.50[a], 0.55[b]
	$NBO_{C15–H15}$	0.56, 0.56[a], 0.60[b]
$NBO_{C5a–C8a}$	$NBO_{C15–H15}$	0.12, 0.12[a], 0.14[b]

[a] For C and H atoms 6-311+G* basis sets were employed.
[b] For C and H atoms 6-311++G** basis sets were employed.

Table 6
Natural charges and natural populations of selected atoms of complex *II*

Atom	Charge	Natural population
H15	0.22085	0.77915
C15	−0.22033	6.22033
H16	0.21547	0.78453
C16	−0.24099	6.24099
H20	0.22038	0.77962
C20	−0.20815	6.20815
H19	0.21675	0.78325
C19	−0.22997	6.22997

5. Conclusions

State of the art DFT computational methods largely overestimate the metal slippage in Rh-Ic complexes. In the case of *anti*-{2,7-dimethyl-*as*-indacene-diide-$[Rh(COD)]_2$} a serious displacement of the ancillary ligands COD from the crystallographic position is found. While the range of available basis sets for rhodium should be expanded and the importance of relativistic effects should be investigated, a possible explanation for the large disagreement is that the conformation of these complexes is ruled by dispersive interactions, which are poorly described by current functionals.

The presence of C–H···C(π) interaction in *anti*-{2,7-dimethyl-*as*-indacene-diide-$[Rh(COD)]_2$} was investigated by second order perturbative NBO analysis. We obtained a meaningful picture of non-covalent interactions between the COD olefin protons and the π electron cloud of the closely adjacent six-membered ring. In particular we found that only the π orbital localised between two specific carbon atoms of the benzene moiety is involved. By comparison with a model complex ethylene–benzene–ethylene we have proved that this asymmetric interaction must be ascribed not only to the distance and orientation of the hydrogen atoms with respect to the benzene ring, but also to the effective electronic density distribution in the *as*-indacene-diide bridging ligand. This has been identified as an edge type π-hydrogen bonding, where the C–H group interacts with only two adjacent carbons of a particular benzene ring. To the best of our knowledge, no theoretical studies have appeared on this kind of contact: the distinction, if any, between a centroid type and an edge type π-hydrogen bonding is still elusive and warrants further study.

Acknowledgments

The authors acknowledge CINECA (Consorzio Interuniversitario di Calcolo del Nord Est, Casalecchio di Reno, Bologna) for the generous allocation of their computational facilities, i.e. the access to IBM SP4. This

work was supported by Universitá degli Studi di Padova (CPDA021354).

Appendix A. Supplementary data

Supplementary data associated with this article can be found, in the online version at doi:10.1016/j.jorganchem.2004.09.078.

References

[1] A. Ceccon, S. Santi, L. Orian, A. Bisello, Coord. Chem. Rev. 248 (7–8) (2004) 683, and references therein.
[2] C. Bonifaci, A. Ceccon, A. Gambaro, F. Manoli, L. Mantovani, P. Ganis, S. Santi, A. Venzo, J. Organomet. Chem. 557 (1) (1998) 97.
[3] A. Bisello, A. Ceccon, A. Gambaro, P. Ganis, F. Manoli, S. Santi, A. Venzo, J. Organomet. Chem. 593–594 (2000) 315.
[4] A. Ceccon, A. Bisello, L. Crociani, A. Gambaro, P. Ganis, F. Manoli, S. Santi, A. Venzo, J. Organomet. Chem. 600 (2000) 94.
[5] A. Ceccon, P. Ganis, F. Manoli, A. Venzo, J. Organomet. Chem. 601 (2000) 267.
[6] S. Santi, A. Ceccon, F. Carli, L. Crociani, A. Bisello, M. Tiso, A. Venzo, Organometallics 21 (13) (2002) 2679.
[7] J.M. Manriquez, M.D. Ward, W.M. Reiff, J.C. Calabrese, N.L. Jones, P.J. Carrolla, E.E. Bunel, J.S. Miller, J. Am. Chem. Soc. 117 (1995) 6182.
[8] P. Roussel, D.R. Cary, S. Barlow, J.C. Green, F. Vartet, D. O'Hare, Organometallics 19 (2000) 1071.
[9] P. Roussel, J.M. Drewitt, D.R. Cary, C.G. Webster, D. O'Hare, J. Chem. Soc., Chem. Commun. (1998) 2055.
[10] D.R. Cary, C.G. Webster, M.J. Drewitt, S. Barlow, J.C. Green, D. O'Hare, J. Chem. Soc., Chem. Commun. (1997) 953.
[11] D.R. Cary, J.C. Green, D. O'Hare, Angew. Chem. Int., Ed. Engl. 36 (1997) 2618.
[12] S. Barlow, D.R. Cary, M.J. Drewitt, D. O'Hare, J. Chem. Soc., Dalton Trans. (1997) 3867.
[13] W.L. Bell, C.J. Curtis, A. Medianer, C.W. Eigenbrot Jr., R. Curtis Haltiwanger, C.G. Pierpont, J.C. Smart, Organometallics 7 (1988) 691.
[14] M.J. Calhorda, L.F. Veiros, Coord. Chem. Rev. 185–186 (1999) 37.
[15] L.F. Veiros, J. Organomet. Chem. 587 (1999) 221.
[16] M.J. Calhorda, L.F. Veiros, J. Organomet. Chem. 635 (2001) 197.
[17] M.J. Calhorda, C.C. Romao, L.F. Veiros, Chem. Eur. J. 8 (2002) 868.
[18] M.J. Calhorda, V. Felix, L.F. Veiros, Coord. Chem. Rev. 230 (2002) 49.
[19] C. Bonifaci, A. Ceccon, S. Santi, C. Mealli, R.W. Zoellner, Inorg. Chim. Acta 240 (1995) 541.
[20] R. Hoffmann, J. Chem. Phys. 39 (1963) 1397.
[21] R.G. Parr, W. Yang, Density Functional Theory of Atoms and Molecules, Oxford University Press, New York, 1989.
[22] M.J. Calhorda, C.A. Gamelas, I.S. Goncalves, E. Herdtweck, C.C. Romao, L.F. Veiros, Organometallics 17 (1998) 2597.
[23] M.J. Calhorda, L.F. Veiros, Inorg. Chim. Acta 350 (2003) 547.
[24] M.T. Garland, J.I. Saillard, I. Chavez, B. Oëlckers, J.M. Manriquez, J. Mol. Struct. (Teochem) 390 (1997) 199.
[25] P. Ganis, A. Ceccon, T. Köhler, F. Manoli, S. Santi, A. Venzo, Inorg. Chem. Commun. 1 (1988) 15.
[26] Y. Kodama, K. Nishihata, M. Nishio, Y. Iitaka, J. Chem. Soc., Perkin Trans. 2 (1976) 1490.
[27] M. Nishio, M. Hirota, Tetrahedron 45 (1989) 7201.
[28] M. Nishio, Y. Umezawa, M. Hirota, Y. Takeuchi, Tetrahedron 51 (1995) 8665.
[29] H. Suezawa, T. Yoshida, Y. Umezawa, S. Tsuboyama, M. Nishio, Eur. J. Inorg. Chem. 12 (2002) 3148.
[30] M. Nishio, M. Hirota, Y. Umezawa, The CH/π Interaction Evidence, Nature and Consequences, Wiley-VCH, New York, 1998.
[31] M. Muraki, Prot. Peptide Lett. 9 (2002) 195.
[32] M. Brandl, M.S. Weiss, A. Jabs, J. Suhnel, R. Hilgenfeld, J. Mol. Biol. 307 (2001) 357.
[33] P. Chakrabarti, U. Samanta, J. Mol. Biol. 251 (1995) 9.
[34] S. Tsuzuki, K. Honda, T. Uchimaru, M. Mikami, K. Tanabe, J. Am. Chem. Soc. 122 (2001) 3746.
[35] P. Tarakeshwar, H.S. Choi, S.J. Lee, K.S. Kim, T.K. Ha, J.H. Jang, J.G. Lee, H. Lee, J. Chem. Phys. 111 (1999) 5838.
[36] P. Tarakeshwar, H.S. Choi, K.S. Kim, J. Am. Chem. Soc. 123 (2001) 3323.
[37] P. Tarakeshwar, K.S. Kim, J. Mol. Struct. 615 (2002) 227.
[38] C. Möller, M.S. Plesset, Phys. Rev. 46 (1934) 618.
[39] J.A. Pople, M. Head-Gordon, K. Raghavachari, J. Chem. Phys. 87 (1987) 5968.
[40] G.E. Scuseria, H.F. Schafer, J. Chem. Phys. 90 (1989) 3700.
[41] J.P. Foster, F. Weinhold, J. Am. Chem. Soc. 102 (1980) 7211.
[42] A.E. Reed, L.A. Curtiss, F. Weinhold, Chem. Rev. 88 (1988) 899.
[43] GAUSSIAN98, Revision A.11.3 M.J. Frisch, G.W. Trucks, H.B. Schlegel, G.E. Scuseria, M.A. Robb, J.R. Cheeseman, V.G. Zakrzewski, J.A. Montgomery Jr., R.E. Stratmann, J.C. Burant, S. Dapprich, J.M. Millam, A.D. Daniels, K.N. Kudin, M.C. Strain, O. Farkas, J. Tomasi, V. Barone, M. Cossi, R. Cammi, B. Mennucci, C. Pomelli, C. Adamo, S. Clifford, J.A. Pople, J. Ochterski, G.A. Petersson, P.Y. Ayala, Q. Cui, K. Morokuma, N. Rega, P. Salvador, J.J. Dannenberg, D.K. Malick, A.D. Rabuck, K. Raghavachari, J.B. Foresman, J. Cioslowski, J.V. Ortiz, A.G. Baboul, B.B. Stefanov, G. Liu, A. Liashenko, P. Piskorz, I. Komaromi, R. Gomperts, R.L. Martin, D.J. Fox, T. Keith, M.A. Al-Laham, C.Y. Peng, A. Nanayakkara, M. Challacombe, P.M.W. Gill, B. Johnson, W. Chen, M.W. Wong, J.L. Andres, C. Gonzalez, M. Head-Gordon, E.S. Replogle, J.A. Pople, Gaussian Inc., Pittsburgh PA, 2002.
[44] A.D. Becke, Phys. Rev. A 38 (1988) 3098.
[45] C. Lee, W. Yang, R.G. Parr, Phys. Rev. B 37 (1988) 785.
[46] P.J. Hay, W.R. Wadt, J. Chem. Phys. 82 (1985) 270.
[47] P.J. Hay, W.R. Wadt, J. Chem. Phys. 82 (1985) 284.
[48] P.J. Hay, W.R. Wadt, J. Chem. Phys. 82 (1985) 299.
[49] Basis sets were obtained from the Extensible Computational Chemistry Environment Basis Set Database, Version 4/17/03, as developed and distributed by the Molecular Science Computing Facility, Environmental and Molecular Sciences Laboratory which is part of the Pacific Northwest Laboratory, P.O. Box 999, Richland, Washington 99352, USA, and funded by the U.S. Department of Energy. The Pacific Northwest Laboratory is a multi-program laboratory operated by Battelle Memorial Institue for the U.S. Department of Energy under contract DE-AC06-76RLO 1830.
[50] NBO 3.1 E.D. Glendening, J.K. Badenhoop, A.D. Reed, J.E. Carpenter, F. Weinhold, Theoretical Chemistry Institute, University of Wisconsin, Madison, WI, 1999.
[51] S.B. Boys, F. Bernardi, Mol. Phys. 19 (1970) 553.
[52] A.K. Kakkar, S.F. Jones, N.J. Taylor, S. Collins, T.B. Marder, J. Chem. Soc., Chem. Commun. (1989) 1454.
[53] E.A. McCullough Jr., E. Aprá, J. Nichols, J. Phys. Chem. A 101 (1997) 2502.
[54] A.K. Kakkar, N.J. Taylor, T.B. Marder, J.K. Shen, N. Hallinan, F. Basolo, Inorg. Chim. Acta 198–200 (1992) 219.
[55] L. Orian, A. Bisello, S. Santi, A. Ceccon, G. Saielli, Chem. Eur. J. 10 (16) (2004) 4029.

[56] F. Jensen, Introduction to Computational Chemistry, Wiley VCH, Great Britain, 2003 (Chapter 6).
[57] S. Harder, Chem. Eur. J. 5 (1999) 1852.
[58] H. Suezawa, T. Yoshida, Y. Umezawa, S. Rsuboyama, M. Nishio, Eur. J. Inorg. Chem. 12 (2002) 3148.
[59] A crystallographic database analysis has revealed the occurrence of two kinds of π-hydrogen contacts, i.e. a centroid type, where the hydrogen atom is directed to the middle of the aromatic ring system, and an edge type where the hydrogen atom makes a close approach to only two adjacent carbons of the ring M.A. Viswamitra, R. Radhakrishnan, J. Bandekar, G.R. Desiraju, J. Am. Chem. Soc. 115 (1993) 4868, and references therein.
[60] K. Nakatsu, H. Yoshioka, K. Kunimoto, T. Kinugasa, S. Ueji, Acta Crystallogr., Sect. B 34 (1978) 2357.
[61] S. Ueji, K. Nakatsu, H. Yoshioka, K. Knioshita, Tetrahedron Lett. 23 (1982) 1173.